Partial vibrational density of states for amorphous solids from inelastic neutron scattering

Dean A. J. Whittaker,[1] Luigi Giacomazzi,[2,3] Devashibhai Adroja,[4,5] Stephen M. Bennington,[4] Alfredo Pasquarello,[2] and Philip S. Salmon[1,*]

[1]*Department of Physics, University of Bath, Bath BA2 7AY, United Kingdom*

[2]*Chaire de Simulation à l'Echelle Atomique, Ecole Polytechnique Fédérale de Lausanne, CH-1015 Lausanne, Switzerland*

[3]*Materials Research Laboratory, University of Nova Gorica, Vipavska 11c, 5270 Ajdovščina, Slovenia*

[4]*ISIS Facility, Rutherford Appleton Laboratory, Chilton, Didcot, Oxon OX11 0QX, United Kingdom*

[5]*Highly Correlated Matter Research Group, Physics Department, University of Johannesburg, P.O. Box 524, Auckland Park 2006, South Africa*

(Received 26 January 2018; revised manuscript received 2 July 2018; published 23 August 2018)

We introduce coherent inelastic neutron scattering with isotope substitution as a technique for measuring site-specific information on the vibrational dynamics of amorphous solids. The technique is used to extract experimentally the *partial* vibrational density of states $G_\alpha(E)$ for both Ge and Se in the prototypical network-forming glass $GeSe_2$, where α specifies the chemical species and E denotes the energy. The efficacy of the approximations used in interpreting the experimental data is validated by using a first-principles model, for which the set of true partial vibrational density of states is directly accessible. Our approach offers an opportunity for exploring accurately the vibrational dynamics of disordered materials.

DOI: 10.1103/PhysRevB.98.064205

I. INTRODUCTION

The vibrational density of states (VDOS) is an essential parameter for describing the collective excitations in amorphous solids, where the absence of translational periodicity precludes their description by using dispersion relations [1,2]. These excitations are important for understanding many of the transport and thermodynamic properties of disordered materials, and govern their interaction with light. For example, the VDOS provides essential information on a variety of thermodynamic properties such as the vibrational contribution to the internal energy, heat capacity, and entropy [3], where the latter is required to find the configurational contribution to the total entropy that is associated with glass relaxation via the Adam-Gibbs formalism [4,5]. It is therefore desirable to maximize the available experimental information by measuring the partial VDOS for each chemical species in a glass. Such site-specific information is accessible for Mössbauer nuclei such as ^{57}Fe by using inelastic x-ray scattering [3]. It has not been forthcoming, however, from coherent inelastic neutron scattering (CINS), which has been a mainstay technique for investigating the dynamics of disordered materials [2,6–10]. A major drawback originates from the employment of the extreme incoherent approximation to analyze CINS spectra, where all of the chemical species are treated as equivalent, which carries clear shortcomings for most materials [6–8].

In this paper, we develop a technique involving CINS with isotope substitution to measure the full set of *partial* VDOS $G_\alpha(E)$ for an amorphous solid, where α denotes the chemical species and E is the energy. The technique is illustrated via its application to glassy $GeSe_2$, a prototype for investigating the effect of network topology on the structure and dynamics of disordered glass-forming materials [11,12]. The efficacy of our experimental approach is examined by generating a first-principles model for which the true partial VDOSs $Z_\alpha(E)$ are known, so that the effect of the approximations used in interpreting the measured spectra can be rigorously tested. From the model it is found that $G_\alpha(E) \simeq Z_\alpha(E)$; that is, the measured functions give an accurate representation of the true partial VDOS for the glass. Our approach goes well beyond that used for extracting structural information on amorphous solids by using neutron diffraction with isotope substitution [13,14].

This paper is organized as follows. In Sec. II we summarize the essential theory leading to the incoherent and extreme incoherent approximations that are made in the analysis of data collected during CINS experiments on amorphous materials. The experimental work is described in Sec. III, and the data analysis procedure is outlined in Sec. IV. The results are presented in Sec. V, and the efficacy of the experimental approach is scrutinized in Sec. VI by employing a first-principles model. Conclusions are drawn in Sec. VII.

II. THEORY

Consider an inelastic neutron scattering experiment on an amorphous solid such as glassy AX_2 that contains N atoms [15,16]. Let $\mathbf{k}_0$ and $\mathbf{k}_1$ denote the incident and scattered neutron wave vectors, respectively, and let 2θ be the scattering angle between them. Let $E_0 = \hbar^2 k_0^2/2m_n$ and $E_1 = \hbar^2 k_1^2/2m_n$ denote the incident and scattered neutron energies, respectively, where $k_0 = |\mathbf{k}_0|$, $k_1 = |\mathbf{k}_1|$, $\hbar$ is the reduced Planck constant, and m_n is the mass of a neutron. The magnitude of the scattering vector $\mathbf{Q} = \mathbf{k}_0 - \mathbf{k}_1$ is given by

$$Q = \sqrt{k_0^2 + k_1^2 - 2k_0 k_1 \cos(2\theta)}, \quad (1)$$

*Corresponding author: p.s.salmon@bath.ac.uk

and the energy transfer

$$E = E_0 - E_1 = \hbar\omega, \tag{2}$$

where ω is an angular frequency. If the nuclear spins and isotopes are randomly distributed over the atoms of each particular element, the double-differential cross section per atom is given by

$$\frac{d^2\sigma}{d\Omega dE} = \frac{1}{N}\frac{k_1}{k_0}\frac{1}{2\pi\hbar}\int_{-\infty}^{\infty} dt\, e^{-i\omega t}\sum_{i=1}^{N}\sum_{j=1}^{N}\overline{b_i b_j} \times \langle e^{-i\mathbf{Q}\cdot\mathbf{R}_i(0)}\, e^{i\mathbf{Q}\cdot\mathbf{R}_j(t)}\rangle, \tag{3}$$

where b_i and b_j are the scattering lengths of nuclei i and j, respectively; $\mathbf{R}_i(0)$ and $\mathbf{R}_j(t)$ are the positions of nuclei i at time $t = 0$ and j at time t, respectively; the brackets $\langle\cdots\rangle$ denote a thermal average; and the bar refers to an average over nuclear spin orientations and isotope distributions.

If there is no correlation between the nuclear spins and particle positions, and no correlation between the isotopes and particle positions, then $\overline{b_i b_j} = \overline{b}^2 + (\overline{b^2} - \overline{b}^2)\delta_{ij}$, where $\overline{b} = (1/N)\sum_i b_i$, $\overline{b^2} = (1/N)\sum_i b_i^2$, and the Kronecker delta $\delta_{ij} = 1$ if $i = j$ or $\delta_{ij} = 0$ if $i \neq j$. The coherent and incoherent contributions to the scattering can then be separated so that

$$\frac{d^2\sigma}{d\Omega dE} = \left.\frac{d^2\sigma}{d\Omega dE}\right|_{\rm coh} + \left.\frac{d^2\sigma}{d\Omega dE}\right|_{\rm inc} = \frac{k_1}{k_0}[S_{\rm coh}(\mathbf{Q}, E) + S_{\rm inc}(\mathbf{Q}, E)]. \tag{4}$$

The coherent total dynamical structure factor

$$S_{\rm coh}(\mathbf{Q}, E) = \frac{1}{N}\frac{\sigma_{\rm coh}}{4\pi}\frac{1}{2\pi\hbar}\int_{-\infty}^{\infty} dt\, e^{-i\omega t}\sum_{i=1}^{N}\sum_{j=1}^{N} \times \langle e^{-i\mathbf{Q}\cdot\mathbf{R}_i(0)} e^{i\mathbf{Q}\cdot\mathbf{R}_j(t)}\rangle, \tag{5}$$

where $\sigma_{\rm coh} = 4\pi\overline{b}^2$, and the incoherent total dynamical structure factor

$$S_{\rm inc}(\mathbf{Q}, E) = \frac{1}{N}\frac{\sigma_{\rm inc}}{4\pi}\frac{1}{2\pi\hbar}\int_{-\infty}^{\infty} dt\, e^{-i\omega t}\sum_{i=1}^{N} \times \langle e^{-i\mathbf{Q}\cdot\mathbf{R}_i(0)} e^{i\mathbf{Q}\cdot\mathbf{R}_i(t)}\rangle, \tag{6}$$

where $\sigma_{\rm inc} = 4\pi(\overline{b^2} - \overline{b}^2) \equiv 4\pi b_{\rm inc}^2$. Coherent scattering involves correlations between either the positions of distinct nuclei at different times or the positions of the same nucleus at different times. Incoherent scattering involves correlations solely between the positions of the same nucleus at different times.

The differential cross section for coherent scattering can be obtained by making the static approximation, where it is assumed that $E_0 \gg |\hbar\omega|$ so that $k_1 \simeq k_0$. Then, on (i) making a distinction between the nuclei of different chemical species and (ii) subtracting the forward scattering, it follows that [13]

$$\left.\frac{d\sigma}{d\Omega}\right|_{\rm coh} = \int_{-\infty}^{E_0}\left.\frac{d^2\sigma}{d\Omega dE}\right|_{\rm coh} dE = F(Q) + \sum_\alpha c_\alpha \overline{b}_\alpha^2, \tag{7}$$

where $F(Q) = \sum_\alpha\sum_\beta c_\alpha c_\beta \overline{b}_\alpha\overline{b}_\beta[S_{\alpha\beta}(Q) - 1]$ is the total structure factor, α and β denote the chemical species, $c_\alpha = N_\alpha/N$ is the atomic fraction of chemical species α, N_α is the number of atoms of chemical species α, $N = \sum_\alpha N_\alpha$, $\overline{b}_\alpha = (1/N_\alpha)\sum_{i\subset\alpha} b_i$ is the coherent neutron scattering length of chemical species α, and $S_{\alpha\beta}(Q)$ is a so-called Faber-Ziman partial structure factor. The differential cross section for incoherent scattering is, within the static approximation, given by

$$\left.\frac{d\sigma}{d\Omega}\right|_{\rm inc} = \int_{-\infty}^{E_0}\left.\frac{d^2\sigma}{d\Omega dE}\right|_{\rm inc} dE = \sum_\alpha c_\alpha \overline{b}_{\alpha,\rm inc}^2, \tag{8}$$

where $\overline{b}_{\alpha,\rm inc}^2 = \overline{b_\alpha^2} - \overline{b}_\alpha^2$ and $\overline{b_\alpha^2} = (1/N_\alpha)\sum_{i\subset\alpha} b_i^2$. The total differential cross section is given by

$$\left.\frac{d\sigma}{d\Omega}\right|_{\rm tot} = \left.\frac{d\sigma}{d\Omega}\right|_{\rm coh} + \left.\frac{d\sigma}{d\Omega}\right|_{\rm inc} = F(Q) + \frac{\sigma_{\rm tot}}{4\pi}, \tag{9}$$

where the total scattering cross section $\sigma_{\rm tot} = 4\pi\sum_\alpha c_\alpha(\overline{b}_\alpha^2 + \overline{b}_{\alpha,\rm inc}^2)$.

A. Multiphonon expansion

Consider an isotropic solid for which each atomic coordinate $\mathbf{R}_i(t)$ can be written in terms of a time-dependent displacement $\mathbf{u}_i(t)$ about a time-independent equilibrium position $\mathbf{R}_i$, such that $\mathbf{R}_i(t) = \mathbf{R}_i + \mathbf{u}_i(t)$. If the displacements are small and harmonic, a multiphonon expansion can be made [16].

In the case of coherent scattering, the multiphonon expansion gives

$$S_{\rm coh}(\mathbf{Q}, E) = \frac{1}{N}\frac{\sigma_{\rm coh}}{4\pi}\sum_{i=1}^{N}\sum_{j=1}^{N}\langle e^{-i\mathbf{Q}\cdot(\mathbf{R}_i-\mathbf{R}_j)}\rangle e^{-[W_i(Q)+W_j(Q)]} \times \frac{1}{2\pi\hbar}\int_{-\infty}^{\infty} dt\, e^{-i\omega t}\sum_{p=0}^{\infty}\frac{1}{p!} \times \langle[\mathbf{Q}\cdot\mathbf{u}_i(0)][\mathbf{Q}\cdot\mathbf{u}_j(t)]\rangle^p, \tag{10}$$

where, for the ith nucleus, $W_i(Q) = (1/6)\langle u_i^2\rangle Q^2$ is the Debye-Waller factor and $\langle u_i^2\rangle$ is the mean-square displacement. In this expansion, $p = 0$ corresponds to elastic scattering, $p = 1$ corresponds to one-phonon scattering, and the remaining terms $p > 1$ correspond to multiphonon scattering. For an isotropic solid it follows that the double-differential cross section for coherent scattering can be written as

$$\left.\frac{d^2\sigma}{d\Omega dE}\right|_{\rm coh} = S_{\rm coh}^{\rm el}(Q)\delta(E) + \frac{k_1}{k_0}[S_{\rm coh,1}(Q, E) + S_{\rm coh,mp}(Q, E)]. \tag{11}$$

The first term describes elastic scattering, and on (i) making a distinction between the nuclei of different chemical species and (ii) subtracting the forward scattering, it gives the differential cross section

$$\left.\frac{d\sigma}{d\Omega}\right|_{\rm coh}^{\rm el} = \int_{-\infty}^{\infty} S_{\rm coh}^{\rm el}(Q)\delta(E)dE = F(Q) + \sum_\alpha c_\alpha \overline{b}_\alpha^2 e^{-2W_\alpha(Q)}, \tag{12}$$

where $W_\alpha(Q)$ is the mean Debye-Waller factor for the atoms of chemical species α. The second term in Eq. (11) describes one-phonon scattering, and in terms of the one-phonon coherent dynamical structure factors $S_{\alpha\beta}(Q, E)$ for chemical species α and β, it follows that

$$S_{\mathrm{coh},1}(Q, E) = \overline{b}_{\mathrm{A}}^2 S_{\mathrm{AA}}(Q, E) + \overline{b}_{\mathrm{X}}^2 S_{\mathrm{XX}}(Q, E) + 2\overline{b}_{\mathrm{A}}\overline{b}_{\mathrm{X}} S_{\mathrm{AX}}(Q, E). \quad (13)$$

The third term in Eq. (11) involves the dynamical structure factor $S_{\mathrm{coh,mp}}(Q, E)$, which describes multiphonon scattering.

In the case of incoherent scattering, the multiphonon expansion gives

$$S_{\mathrm{inc}}(\mathbf{Q}, E) = \frac{1}{N}\frac{\sigma_{\mathrm{inc}}}{4\pi}\sum_{i=1}^{N} e^{-2W_i(Q)}\frac{1}{2\pi\hbar}\int_{-\infty}^{\infty} dt\, e^{-i\omega t}\sum_{p=0}^{\infty}\frac{1}{p!} \times \langle[\mathbf{Q}\cdot\mathbf{u}_i(0)][\mathbf{Q}\cdot\mathbf{u}_i(t)]\rangle^p. \quad (14)$$

Again, $p = 0$ corresponds to elastic scattering, $p = 1$ corresponds to one-phonon scattering, and the remaining terms $p > 1$ correspond to multiphonon scattering. For an isotropic solid it follows that the double-differential cross section for incoherent scattering can be written as

$$\left.\frac{d^2\sigma}{d\Omega dE}\right|_{\mathrm{inc}} = S_{\mathrm{inc}}^{\mathrm{el}}(Q)\delta(E) + \frac{k_1}{k_0}[S_{\mathrm{inc},1}(Q, E) + S_{\mathrm{inc,mp}}(Q, E)]. \quad (15)$$

The first term describes elastic scattering and gives the differential cross section

$$\left.\frac{d\sigma}{d\Omega}\right|_{\mathrm{inc}}^{\mathrm{el}} = \int_{-\infty}^{\infty} S_{\mathrm{inc}}^{\mathrm{el}}(Q)\delta(E)dE = \sum_\alpha c_\alpha \overline{b}_{\alpha,\mathrm{inc}}^2 e^{-2W_\alpha(Q)}. \quad (16)$$

The dynamical structure factor $S_{\mathrm{inc},1}(Q, E)$ describes one-phonon scattering, and in terms of the one-phonon incoherent dynamical structure factors $S_{\alpha,\mathrm{inc}}(Q, E)$ for chemical species α, it follows that

$$S_{\mathrm{inc},1}(Q, E) = \overline{b}_{\mathrm{A,inc}}^2 S_{\mathrm{A,inc}}(Q, E) + \overline{b}_{\mathrm{X,inc}}^2 S_{\mathrm{X,inc}}(Q, E). \quad (17)$$

The dynamical structure factor $S_{\mathrm{inc,mp}}(Q, E)$ describes multiphonon scattering.

The general motion of N quantized simple harmonic oscillators in three dimensions arising from single-phonon processes can be described by the superposition of $3N$ normal modes. Within the framework of a normal-mode analysis, the incoherent dynamical structure factors can be written as

$$S_{\alpha,\mathrm{inc}}(Q, E) = \frac{\hbar^2 Q^2}{2M_\alpha} e^{-2W_\alpha(Q)}\frac{\langle n(E)+1\rangle}{E} Z_\alpha(E). \quad (18)$$

Here, M_α is the nuclear mass of chemical species α; $\langle n(E)\rangle = [\exp(E/k_{\mathrm{B}}T) - 1]^{-1}$ is the Bose occupation factor at absolute temperature T, and the displacement-weighted partial VDOS for chemical species α is given by

$$Z_\alpha(E) = \frac{1}{3N}\sum_{\alpha i=1}^{N_\alpha}\sum_{\nu=1}^{3N} |\mathbf{e}_{\alpha i}^{\nu}|^2 \delta(|E| - E_\nu), \quad (19)$$

where $\mathbf{e}_{\alpha i}^{\nu}$ is the displacement vector of the ith nucleus of chemical species α in the νth normal mode and E_ν is the energy of that mode. The partial VDOS is normalized so that

$$\int_0^{E_{\max}} Z_\alpha(E)dE = c_\alpha, \quad (20)$$

where $E_{\max}$ corresponds to the maximum energy of a normal mode.

For neutron energy loss, i.e., when $E > 0$ and a single phonon is created, the corresponding incoherent dynamical structure factor $S_{\alpha,\mathrm{inc}+1}(Q, E)$ is given by Eq. (18) with

$$\langle n(E)+1\rangle = \exp(E/k_{\mathrm{B}}T)/[\exp(E/k_{\mathrm{B}}T) - 1]. \quad (21)$$

For neutron energy gain, i.e., when $E < 0$ and a single phonon is annihilated, the corresponding incoherent dynamical structure factor $S_{\alpha,\mathrm{inc}-1}(Q, E)$ is given by Eq. (18) with

$$\frac{\langle n(E)+1\rangle}{E} = -\frac{1}{|E|}\frac{\exp[-|E|/k_{\mathrm{B}}T]}{[\exp(-|E|/k_{\mathrm{B}}T) - 1]} = \frac{\langle n(|E|)\rangle}{|E|}. \quad (22)$$

At low temperatures, $\langle n(|E|)\rangle \simeq 0$ for neutron energy gain, and $\langle n(E)+1\rangle \simeq 1$ for neutron energy loss; that is, the single-phonon scattering will be dominated by $S_{\alpha,\mathrm{inc}+1}(Q, E)$.

In the *extreme* incoherent approximation no distinction is made between the different nuclei; that is, they are all assumed to have the same incoherent scattering length b_{inc}, the same nuclear mass M, and the same Debye-Waller factor $W(Q)$. The dynamical structure factor for one-phonon scattering becomes

$$S_{\mathrm{inc},1}(Q, E) = b_{\mathrm{inc}}^2 \frac{\hbar^2 Q^2}{2M} e^{-2W(Q)}\frac{\langle n(E)+1\rangle}{E} Z(E), \quad (23)$$

where $Z(E)$ is the total VDOS. For a sample of glassy AX_2 containing $N = N_{\mathrm{A}} + N_{\mathrm{X}}$ atoms, the total VDOS is given by

$$Z(E) = Z_{\mathrm{A}}(E) + Z_{\mathrm{X}}(E) = \frac{1}{3N}\sum_{\nu=1}^{3N}\delta(|E| - E_\nu), \quad (24)$$

where the last equality follows from the normalization condition $\sum_{i=1}^{N}|\mathbf{e}_i^\nu|^2 = \sum_{\mathrm{A}i=1}^{N_{\mathrm{A}}}|\mathbf{e}_{\mathrm{A}i}^\nu|^2 + \sum_{\mathrm{X}i=1}^{N_{\mathrm{X}}}|\mathbf{e}_{\mathrm{X}i}^\nu|^2 = 1$. The total VDOS is normalized so that

$$\int_0^{E_{\max}} Z(E)dE = 1. \quad (25)$$

In practice, the incoherent scattering lengths, masses, and Debye-Waller factors of all the nuclei will not be identical. Then, the dynamical structure factor for one-phonon scattering is often estimated by replacing b_{inc}^2, M, and $W(Q)$ in Eq. (23) by the mean values $\langle b_{\mathrm{inc}}^2\rangle = \sum c_\alpha \overline{b}_{\alpha,\mathrm{inc}}^2$, $\overline{M} = \sum c_\alpha M_\alpha$, and $\overline{W}(Q) = \sum c_\alpha W_\alpha(Q)$, respectively. The total VDOS in the resultant expression is then an approximation of the true total VDOS.

Within the extreme incoherent approximation, the overall dynamical structure factor for inelastic incoherent scattering in Eq. (15) can be rewritten as [17,18]

$$S_{\mathrm{inc}}(Q, E) \equiv S_{\mathrm{inc},1}(Q, E) + S_{\mathrm{inc,mp}}(Q, E) = \langle b_{\mathrm{inc}}^2\rangle e^{-2\overline{W}(Q)}\sum_{p=1}^{\infty}\frac{1}{p!}\left(\frac{\hbar^2 Q^2}{2\overline{M}}\right)^p u_p(E). \quad (26)$$

In this equation, the dynamical structure factor for one-phonon scattering corresponds to $p = 1$, where

$$u_1(E) = \langle n(E) + 1 \rangle \frac{Z(E)}{E}, \tag{27}$$

and the dynamical structure factor for multiphonon scattering corresponds to the remaining terms for which $p > 1$, where $u_p(E)$ is given by the convolution relation

$$u_p(E) = \int_{-\infty}^{\infty} u_{p-1}(E')u_1(E - E')dE'. \tag{28}$$

B. Incoherent approximation for coherent scattering

Consider the case when the incoherent scattering from a sample of, e.g., glassy AX_2 is negligibly small. A generalized partial VDOS can still be accessed by making the so-called incoherent approximation where it is assumed that only those correlations involving the same nuclei ($i = j$) contribute towards the coherent dynamical structure factors. The term $S_{\mathrm{AX}}(Q, E)$ describes distinct nuclei and therefore vanishes from Eq. (13), so that

$$S_{\mathrm{coh},1}(Q, E) = \overline{b}_{\mathrm{A}}^2 S_{\mathrm{AA}}(Q, E) + \overline{b}_{\mathrm{X}}^2 S_{\mathrm{XX}}(Q, E), \tag{29}$$

where the partial dynamical structure factors for one-phonon scattering can be written as

$$S_{\alpha\alpha}(Q, E) = \frac{\hbar^2 Q^2}{2M_\alpha} e^{-2W_\alpha(Q)} \frac{\langle n(E) + 1 \rangle}{E} G_\alpha(Q, E). \tag{30}$$

This equation defines a generalized partial VDOS $G_\alpha(Q, E)$ for chemical species α, which gives an account of the distinct-particle correlations that are neglected within the incoherent approximation [19]. The corresponding partial VDOS follows from the average

$$G_\alpha(E) = \frac{1}{Q_{\max} - Q_{\min}} \int_{Q_{\min}}^{Q_{\max}} G_\alpha(Q, E)dQ, \tag{31}$$

where $Q_{\min}$ and $Q_{\max}$ are the minimum and maximum scattering vectors accessed by experiment when E is the energy transfer.

In the present work on glassy $GeSe_2$ we adopt this approach, where only self-particle motions contribute towards the coherent scattering, and apply the method of CINS with isotope substitution to samples of glassy ^{70}Ge $^{\mathrm{N}}$Se$_2$, $^{\mathrm{N}}$Ge $^{\mathrm{N}}$Se$_2$, and ^{73}Ge ^{76}Se$_2$, where N denotes the natural isotopic abundance. If the corresponding partial dynamical structure factors for one-phonon scattering are denoted by ${}^{70}_{\mathrm{N}}S_{\mathrm{coh},1}(Q, E)$, ${}^{\mathrm{N}}_{\mathrm{N}}S_{\mathrm{coh},1}(Q, E)$, and ${}^{73}_{76}S_{\mathrm{coh},1}(Q, E)$, respectively, it follows that

$$\begin{bmatrix} {}^{70}_{\mathrm{N}}S_{\mathrm{coh},1}(Q, E) \\ {}^{\mathrm{N}}_{\mathrm{N}}S_{\mathrm{coh},1}(Q, E) \\ {}^{73}_{76}S_{\mathrm{coh},1}(Q, E) \end{bmatrix} = \begin{bmatrix} \overline{b}^2_{^{70}\mathrm{Ge}}/M_{^{70}\mathrm{Ge}} & \overline{b}^2_{^{\mathrm{N}}\mathrm{Se}}/M_{^{\mathrm{N}}\mathrm{Se}} \\ \overline{b}^2_{^{\mathrm{N}}\mathrm{Ge}}/M_{^{\mathrm{N}}\mathrm{Ge}} & \overline{b}^2_{^{\mathrm{N}}\mathrm{Se}}/M_{^{\mathrm{N}}\mathrm{Se}} \\ \overline{b}^2_{^{73}\mathrm{Ge}}/M_{^{73}\mathrm{Ge}} & \overline{b}^2_{^{76}\mathrm{Se}}/M_{^{76}\mathrm{Se}} \end{bmatrix} \times \begin{bmatrix} S'_{\mathrm{GeGe}}(Q, E) \\ S'_{\mathrm{SeSe}}(Q, E) \end{bmatrix}, \tag{32}$$

where $S'_{\alpha\alpha}(Q, E) \equiv M_\alpha S_{\alpha\alpha}(Q, E)$. This overconditioned set of equations can be solved by using the method of singular-value decomposition [20].

The validity of the approximations leading to Eqs. (29)–(32) has not been ascertained and will discussed in Sec. VI.

C. Extreme incoherent approximation for coherent scattering

In contrast to the approach given in Sec. II B, it is usual to make the *extreme* incoherent approximation when performing inelastic neutron scattering experiments on coherently scattering glassy materials [6,7]. Here, all nuclei are assumed to have the same mean-square scattering length $\langle \overline{b}^2 \rangle = \sum c_\alpha \overline{b}_\alpha^2$, the same nuclear mass $\overline{M} = \sum c_\alpha M_\alpha$, and the same Debye-Waller factor $\overline{W}(Q) = \sum c_\alpha W_\alpha(Q)$. Then, Eq. (29) is rewritten as

$$S_{\mathrm{coh},1}(Q, E) = \langle \overline{b}^2 \rangle \frac{\hbar^2 Q^2}{2\overline{M}} e^{-2\overline{W}(Q)} \frac{\langle n(E) + 1 \rangle}{E} G_1(Q, E), \tag{33}$$

which delivers the generalized total VDOS for one-phonon scattering $G_1(Q, E)$ [19]. The effective total VDOS for one-phonon scattering follows from the average

$$G_1(E) = \frac{1}{Q_{\max} - Q_{\min}} \int_{Q_{\min}}^{Q_{\max}} G_1(Q, E)dQ. \tag{34}$$

In this approach, the effect of the approximations on $G_1(E)$ is obscured, and the contributions to the dynamics from different chemical species are unknown.

Similarly, the overall dynamical structure factor for inelastic coherent scattering in Eq. (11) can be written as

$$S_{\mathrm{coh}}(Q, E) \equiv S_{\mathrm{coh},1}(Q, E) + S_{\mathrm{coh,mp}}(Q, E) \tag{35}$$

$$= \langle \overline{b}^2 \rangle \frac{\hbar^2 Q^2}{2\overline{M}} e^{-2\overline{W}(Q)} \frac{\langle n(E) + 1 \rangle}{E} G(Q, E), \tag{36}$$

where $G(Q, E) = G_1(Q, E) + G_{\mathrm{mp}}(Q, E)$ and $G_{\mathrm{mp}}(Q, E)$ is the multiphonon contribution. Hence, the corresponding effective VDOS

$$G(E) = G_1(E) + G_{\mathrm{mp}}(E) = \frac{1}{Q_{\max} - Q_{\min}} \int_{Q_{\min}}^{Q_{\max}} G(Q, E)dQ \tag{37}$$

has contributions from both single- and multiphonon scattering events, where

$$G_{\mathrm{mp}}(E) = \frac{1}{Q_{\max} - Q_{\min}} \int_{Q_{\min}}^{Q_{\max}} G_{\mathrm{mp}}(Q, E)dQ. \tag{38}$$

We note that, within the extreme incoherent approximation, the dynamical structure factor can be approximated by the expression [see Eq. (26)]

$$S_{\mathrm{coh}}(Q, E) \simeq \langle \overline{b}^2 \rangle e^{-2\overline{W}(Q)} \sum_{p=1}^{\infty} \frac{1}{p!} \left(\frac{\hbar^2 Q^2}{2\overline{M}} \right)^p u_p(E), \tag{39}$$

where, by comparing Eqs. (36) and (39), it follows that

$$G(Q, E) \simeq \frac{E}{\langle n(E) + 1 \rangle} \sum_{p=1}^{\infty} \frac{1}{p!} \left(\frac{\hbar^2 Q^2}{2\overline{M}} \right)^{p-1} u_p(E). \tag{40}$$

Here, the one-phonon contribution to $G(Q, E)$ is given by the $p = 1$ term, i.e.,

$$G_1(Q, E) \simeq \frac{E}{\langle n(E)+1\rangle} u_1(E), \tag{41}$$

where $u_1(E)$ is given by Eq. (27). The multiphonon contribution to $G(Q, E)$ is given by the remaining terms for which $p > 1$, i.e.,

$$G_{\rm mp}(Q, E) \simeq \frac{E}{\langle n(E)+1\rangle} \sum_{p=2}^{\infty} \frac{1}{p!} \left(\frac{\hbar^2 Q^2}{2\overline{M}}\right)^{p-1} u_p(E), \tag{42}$$

where the terms $u_p(E)$ $(p > 1)$ are given by Eq. (28).

Equation (39) can be used to estimate the multiphonon contribution to $S_{\rm coh}(Q, E)$. Then, the one-phonon dynamical structure factor is given by

$$S_{\rm coh,1}(Q, E) = S_{\rm coh}(Q, E) - S_{\rm coh,mp}(Q, E), \tag{43}$$

where

$$S_{\rm coh,mp}(Q, E) = \langle \overline{b}^2 \rangle e^{-2\overline{W}(Q)} \sum_{p=2}^{\infty} \frac{1}{p!} \left(\frac{\hbar^2 Q^2}{2\overline{M}}\right)^{p} u_p(E). \tag{44}$$

D. Differential cross section and the Debye-Waller factor

In an inelastic neutron scattering experiment, the elastic and inelastic contributions to the measured signal can be separated. For the elastic contribution, it follows from Eqs. (12) and (16) that the total differential cross section is given by

$$\left.\frac{d\sigma}{d\Omega}\right|_{\rm tot}^{\rm el} = \left.\frac{d\sigma}{d\Omega}\right|_{\rm coh}^{\rm el} + \left.\frac{d\sigma}{d\Omega}\right|_{\rm inc}^{\rm el} = F(Q) + \sum_{\alpha} c_\alpha \left(\overline{b}_\alpha^2 + \overline{b}_{\alpha,\rm inc}^2\right) e^{-2W_\alpha(Q)}. \tag{45}$$

If the different chemical species have the same Debye-Waller factor, i.e., $W_{\rm A}(Q) = W_{\rm X}(Q) = \overline{W}(Q)$, it follows that $d\sigma/d\Omega|_{\rm tot}^{\rm el} = F(Q) + (\sigma_{\rm tot}/4\pi)e^{-2\overline{W}(Q)}$. By comparison, in a diffraction experiment the measured total differential cross section $d\sigma/d\Omega|_{\rm tot}$ is given by Eq. (9), where $\sigma_{\rm tot}$ is not weighted by a term involving the Q-dependent Debye-Waller factor. Hence, $\overline{W}(Q)$ can be extracted by comparing $d\sigma/d\Omega|_{\rm tot}^{\rm el}$ from an inelastic neutron scattering experiment with $d\sigma/d\Omega|_{\rm tot}$ from a neutron diffraction experiment.

III. EXPERIMENT

Inelastic neutron scattering experiments were performed on isotopically enriched samples of glassy $GeSe_2$ [21,22] using the high-count-rate spectrometer MERLIN at the ISIS pulsed neutron source [23] with an incident neutron energy $E_0 = 59.5(1)$ meV, which gives an energy resolution function for elastic scattering of full width at half maximum $\Delta E = 3.65$ meV. Each sample was loaded into a thin-walled annular container made from Al foil within a He-filled glove box, and the container was suspended at the end of the cooling stick of a closed-cycle refrigerator. Measurements were made at a temperature of 5 K for each sample within its container and for an empty container. A low temperature was used to suppress (i) anharmonic motion and (ii) the multiphonon contribution to the measured signal. A measurement was also made for a cylindrical vanadium standard.

The coherent neutron scattering lengths, taking into account the isotopic enrichments, are $\overline{b}_{^{70}\rm Ge} = 10.0(1)$, $\overline{b}_{^{\rm N}\rm Ge} = 8.185(20)$, and $\overline{b}_{^{73}\rm Ge} = 5.09(4)$ fm versus $\overline{b}_{^{76}\rm Se} = 12.2(1)$ and $\overline{b}_{^{\rm N}\rm Se} = 7.970(9)$ fm [24]. Incoherent scattering was neglected because its cross section for the different isotopically enriched $GeSe_2$ glasses is $< 4\%$ of the coherent scattering cross section.

IV. DATA ANALYSIS PROCEDURE

Let $I_{\rm sc}^{\rm E}(Q, E)$ denote the measured intensity for the sample in its container, and let $I_{\rm c}^{\rm E}(Q, E)$ denote the measured intensity for the empty container, where the measured time-of-flight spectra for each scattering angle 2θ have been converted to the variables Q and E and have been placed on a common scale by reference to the scattering from the vanadium standard [25]. The scattering from the bare sample can be approximated by the expression

$$I_{\rm s}(Q, E) = \frac{m}{A_{\rm sc,sc}(Q, E)} \left[I_{\rm sc}^{\rm E}(Q, E) - I_{\rm c}^{\rm E}(Q, E)\right], \tag{46}$$

where $A_{\rm sc,sc}(Q, E)$ is the attenuation coefficient for scattering by the sample and container that is attenuated (through absorption and scattering) by the presence of the sample and container [26]. The normalization constant m ensures that the intensity is placed on an absolute scale such that $\int I_{\rm s}(Q, E)dE \simeq d\sigma/d\Omega|_{\rm tot}$, where the differential cross section is given by Eq. (9).

In practice, Eq. (46) will not lead to an elimination of the signal from multiple scattering. If the multiple scattering is assumed to be isotropic, then for the (Q, E) region of the measured spectra where resolution-broadened elastic scattering cannot be observed, $I_{\rm s}(Q, E)$ at fixed energy transfer E can be fitted to the expression

$$I_{\rm s}^{\rm fit}(Q, E) = I_{\rm ms}(E) + B(E)Q^2 \exp[-2\overline{W}(Q)]. \tag{47}$$

Here, $I_{\rm ms}(E)$ is an estimate of the multiple-scattering contribution to $I_{\rm s}(Q, E)$, and the second term originates from making the extreme incoherent approximation for $S_{\rm coh,1}(Q, E)$ and neglecting the Q dependence of $G_1(Q, E)$ [see Eq. (33)]. The residual contribution from multiple scattering can be obtained for each energy transfer E by using $I_{\rm ms}(E)$ and $B(E)$ as fitting parameters [27].

Last, the multiphonon contribution to the scattering can be estimated by using an iterative procedure [17,18], where $G(E)$ is calculated from the measured data using Eq. (37) and the effective VDOS for single-phonon scattering is obtained from the expression

$$G_1^{(i+1)}(E) = G(E) - G_{\rm mp}^{(i)}(E), \tag{48}$$

where i $(= 1, 2, 3, \dots)$ denotes a step in the iterative procedure. In the first iteration, $u_1(E)$ is calculated using Eq. (27) by assuming that $Z(E) = G_1^{(1)}(E) = G(E)$; the $u_p(E)$ $(p > 1)$ terms are then calculated using Eq. (28) to give $G_{\rm mp}^{(1)}(Q, E)$ from Eq. (42), and $G_{\rm mp}^{(1)}(E)$ follows from Eq. (38). In the second iteration, a new estimate $G_1^{(2)}(E) = G(E) - G_{\rm mp}^{(1)}(E)$ for $Z(E)$ is provided by Eq. (48), which is used to obtain revised estimates for $u_1(E)$ and the $u_p(E)$ $(p > 1)$ terms, thereby

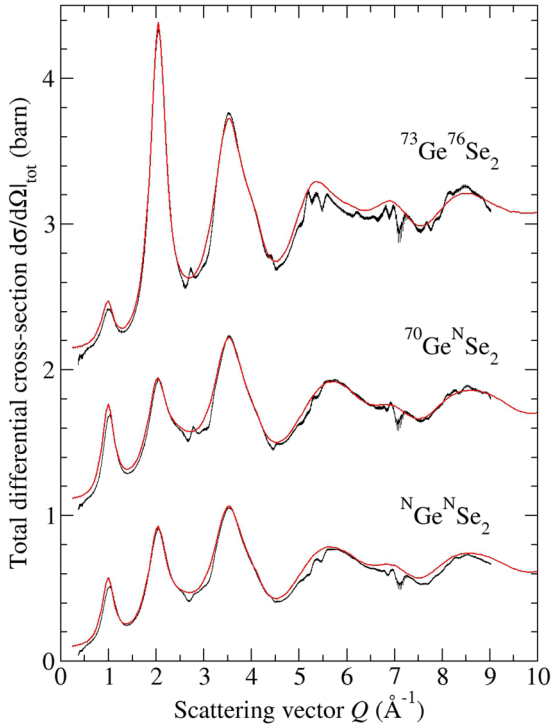

FIG. 1. The total differential cross section $d\sigma/d\Omega|_{\rm tot} = F(Q) + \sigma_{\rm tot}/4\pi$ for different isotopically enriched samples of vitreous $GeSe_2$ as obtained (i) from $I_s(Q, E)$ at 5 K by integrating over the energy range accessible to the MERLIN spectrometer ($-50\,{\rm meV} \leqslant E \leqslant 50\,{\rm meV}$) at a given value of Q (black curves with vertical error bars) or (ii) from neutron diffraction experiments on the same samples at 299(1) K (solid red curves) [21,22]. For clarity of presentation, the curves for $^{70}Ge\,^{N}Se_2$ and $^{73}Ge^{76}Se_2$ are shifted vertically by 1 and 2 barns, respectively.

delivering $G^{(2)}_{\rm mp}(Q, E)$ and $G^{(2)}_{\rm mp}(E)$. The starting point for the third iteration is provided by $G^{(3)}_1(E) = G(E) - G^{(2)}_{\rm mp}(E)$. At the end of each iteration, $G^{(i+1)}_1(E)$ is compared to $G^{(i)}_1(E)$, and unless the convergence criterion $G^{(i+1)}_1(E) = G^{(i)}_1(E)$ is achieved, the iterative procedure is continued. On convergence at step $i + 1$, the final multiphonon contribution to the effective VDOS is given by $G^{(i)}_{\rm mp}(E)$; the multiphonon contribution to the dynamical structure factor $S_{\rm coh,mp}(Q, E)$ can be calculated from Eq. (44), and the single-phonon dynamical structure factor $S_{\rm coh,1}(Q, E)$ follows from Eq. (43).

The multiphonon correction was tested by using model data sets typical of those measured for glassy $GeSe_2$, with $u_p(E)$ calculated to the fifth phonon ($p = 5$) term [28]. Typically, convergence was achieved after a small number of iterations with $i = 3$.

V. RESULTS

Figure 1 shows that the CINS data sets for glassy $^{70}Ge\,^{N}Se_2$, $^{N}Ge^{N}Se_2$, and $^{73}Ge^{76}Se_2$ integrate to give an excellent account of the total differential cross sections $d\sigma/d\Omega|_{\rm tot} = F(Q) + \sigma_{\rm tot}/4\pi$ as measured using diffraction [22]. The contrast between these cross sections originates from differences between the coherent neutron scattering lengths of the Ge and Se isotopes (Sec. III).

The Debye-Waller factor was measured by using MERLIN to perform an additional CINS experiment on glassy $^{N}Ge^{N}Se_2$ but with $E_0 = 29.9(1)$ meV, which gives improved resolution of the elastic line ($\Delta E = 1.59$ meV). Then, $d\sigma/d\Omega|_{\rm tot}$ was compared to the total differential cross section for elastic scattering $d\sigma/d\Omega|^{\rm el}_{\rm tot} = F(Q) + (\sigma_{\rm tot}/4\pi)\exp[-2\overline{W}(Q)]$, wherein the Debye-Waller factors for Ge and Se are assumed to be the same, i.e., $W_{\rm Ge}(Q) = W_{\rm Se}(Q) = \overline{W}(Q)$ (Sec. II D). The corresponding mean-square atomic displacement $\langle u^2\rangle/3 = 2\overline{W}(Q)/Q^2 = 0.002(1)\text{Å}^2$ at 11(1) K, which compares to $\langle u^2\rangle/3 = 0.00188\,\text{Å}^2$ at 13(2) K from previous work [29].

Figure 2 shows contour plots of the measured $G_1(Q, E)$ functions for the different isotopically enriched samples, as obtained by making the extreme incoherent approximation (Sec. II C). The results show three energy bands at ~10.9, 26.5, and 36.7 meV with peaks at various Q values (Table I). The peak intensity for the band at ~36.7 meV increases with the coherent scattering length for Ge (see Sec. III) and is largest for glassy $^{70}Ge\,^{N}Se_2$. In comparison, the peak intensity for the band at ~10.9 meV increases with the coherent scattering length for Se and is largest for glassy $^{73}Ge^{76}Se_2$. The feature at $Q \sim 3.0\,\text{Å}^{-1}$ and $E \sim 10.9$ meV shows structure that is most evident for glassy $^{73}Ge^{76}Se_2$. The first-principles model (see Sec. VI) suggests that this structure originates from two peaks at Q values of ~3.1 and ~1.9 Å^{-1}, with a separation in energy of ~2.5 meV. The dissimilarity between the contour plots for glassy $^{70}Ge\,^{N}Se_2$ and $^{73}Ge\,^{76}Se_2$ originates from a breakdown of the extreme incoherent approximation: Although the masses of the Ge and Se isotopes are similar, there is contrast between the coherent neutron scattering lengths with $\bar{b}_{^{70}\rm Ge} > \bar{b}_{^{N}\rm Se}$ and $\bar{b}_{^{73}\rm Ge} < \bar{b}_{^{76}\rm Se}$. In contrast, $\bar{b}_{^{N}\rm Ge} \simeq \bar{b}_{^{N}\rm Se}$, so the total effective VDOS $G_1(E)$ obtained from $G_1(Q, E)$ for the $^{N}Ge^{N}Se_2$ sample (see Fig. 3) should give a good approximation of the total effective VDOS $G_{\rm tot}(E) = G_{\rm Ge}(E) + G_{\rm Se}(E)$ (see below). The peaks in $G_1(E)$ originate from the energy bands in $G_1(Q, E)$ at ~10.9, 26.5, and 36.7 meV.

Figure 4 shows contour plots of the measured generalized partial VDOS $G_{\rm Ge}(Q, E)$ and $G_{\rm Se}(Q, E)$, as obtained by using the method of singular-value decomposition to solve Eq. (32). These plots show significant differences; for example, there is an energy band in $G_{\rm Se}(Q, E)$ at ~26.8 meV that is suppressed in $G_{\rm Ge}(Q, E)$ and therefore originates predominantly from the motion of Se atoms. Such information cannot be backed out from any of the individual $G_1(Q, E)$ functions presented in Fig. 2: It is necessary to use the method of CINS with isotope substitution to measure the $G_\alpha(Q, E)$ functions. The associated averages $\langle G_\alpha(Q, E)\rangle = \int_{E_1}^{E_2} G_\alpha(Q, E)\,dE/(E_2 - E_1)$ are shown in Fig. 5 for energy ranges corresponding to the first three peaks in $G_1(E)$, where the $G_\alpha(Q, E)$ functions are averaged in order to reduce the statistical error. The peaks in $G_\alpha(Q, E)$ manifest themselves as oscillations in $\langle G_\alpha(Q, E)\rangle$.

Figure 6 shows the measured $G_\alpha(E)$ functions, as obtained by averaging $G_\alpha(Q, E)$ over Q according to Eq. (31). Figure 3 shows the sum $G_{\rm tot}(E) = G_{\rm Ge}(E) + G_{\rm Se}(E)$, which is compared to the $G_1(E)$ functions obtained in the present

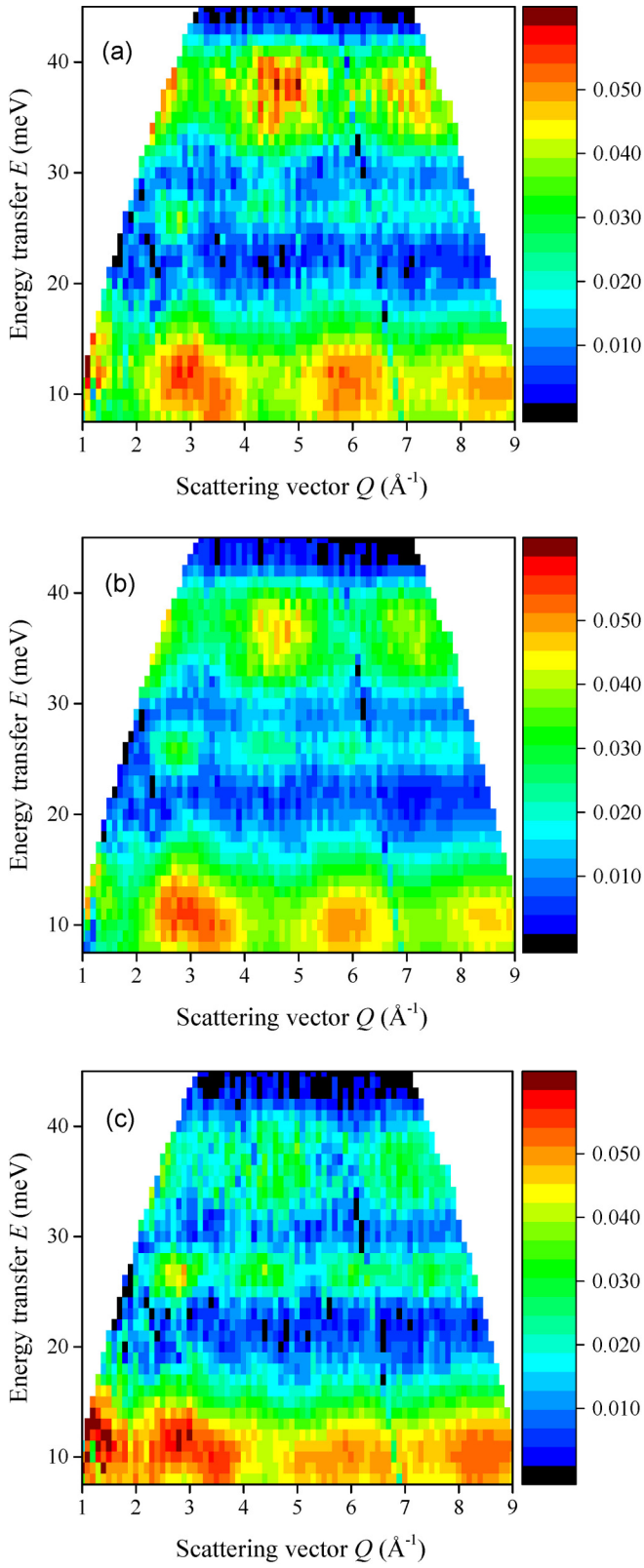

FIG. 2. Contour plots of the measured $G_1(Q, E)$ functions for vitreous (a) ^{70}Ge ^{N}Se$_2$, (b) ^{N}Ge^{N}Se$_2$, and (c) ^{73}Ge^{76}Se$_2$.

and previous [29,30] work by analyzing the measured CINS spectra for glassy ^{N}Ge^{N}Se$_2$ within the extreme incoherent approximation. As discussed above, $G_1(E)$ should give a good approximation to $G_{\rm tot}(E)$, which is confirmed by the experimental results. In this respect, glassy ^{N}Ge^{N}Se$_2$ is atypical: The extreme incoherent approximation does not hold for most amorphous solids, including generic network-forming glasses such as SiO_2 and GeO_2.

TABLE I. The measured Q-space peak positions Q_n ($n = 1, 2, 3,$ or 4) for the energy bands centered at $\langle E\rangle$ in the $G_1(Q, E)$ functions shown in Fig. 2 for glassy ^{70}Ge ^{N}Se$_2$, ^{N}Ge^{N}Se$_2$, and ^{73}Ge^{76}Se$_2$ and the $G_\alpha(Q, E)$ functions shown in Fig. 4.

$\langle E\rangle$ (meV)	Q_1 (Å^{-1})	Q_2 (Å^{-1})	Q_3 (Å^{-1})	Q_4 (Å^{-1})
		$G_1(Q, E)$ for ^{70}Ge ^{N}Se$_2$		
11.3(5)	3.0(2)	5.9(2)	8.4(2)	
26.7(5)	2.7(2)	4.4(2)	6.1(2)	7.4(5)
37.6(5)		4.7(2)	6.9(2)	
		$G_1(Q, E)$ for ^{N}Ge ^{N}Se$_2$		
10.6(5)	3.0(2)	5.8(2)	8.5(2)	
26.0(5)	2.7(2)	4.4(2)	5.9(2)	7.7(2)
36.2(5)		4.7(2)	7.0(2)	
		$G_1(Q, E)$ for ^{73}Ge ^{76}Se$_2$		
10.8(5)	2.9(2)	5.9(2)	8.3(2)	
26.7(5)	2.7(2)	4.4(2)	6.0(2)	7.4(2)
36.4(5)		4.7(2)	6.9(2)	
		$G_{\rm Ge}(Q, E)$		
11.4(5)	3.1(2)	5.7(2)	8.4(2)	
37.3(5)		4.5(2)	7.2(2)	
		$G_{\rm Se}(Q, E)$		
10.7(5)	2.9(2)	6.0(2)	8.2(2)	
26.8(5)	2.7(2)	4.4(2)	6.2(2)	7.5(2)
36.1(5)		4.5(2)	6.9(2)	

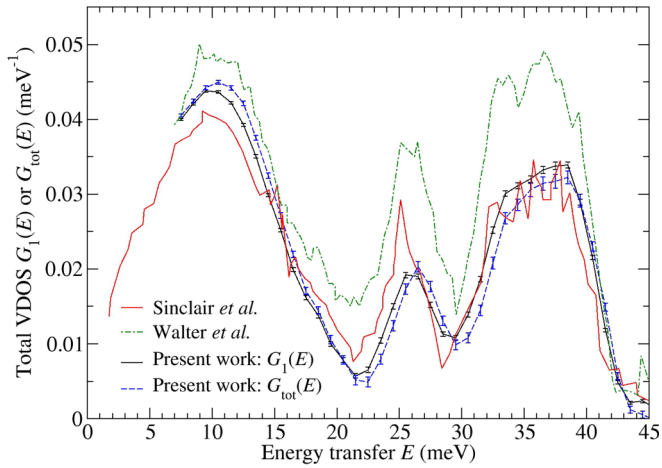

FIG. 3. The $G_1(E)$ functions measured using CINS for vitreous ^{N}Ge^{N}Se$_2$ in the present work at 5 K (solid black curve with vertical error bars), in the work by Walter *et al.* [29] at 13(2) K (dash-dotted green curve), and in the work by Sinclair *et al.* [30] at 18(1) K (solid red curve). The results are compared to the sum $G_{\rm tot}(E) = G_{\rm Ge}(E) + G_{\rm Se}(E)$ (dashed blue curve with vertical error bars).

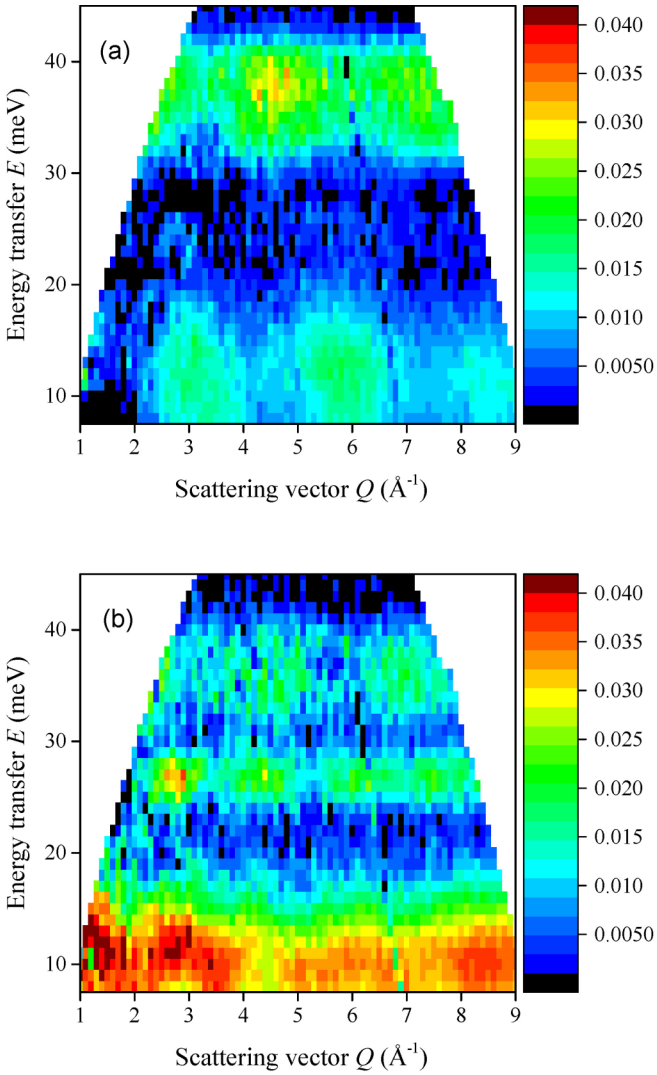

FIG. 4. Contour plots of the measured $G_\alpha(Q, E)$ functions for (a) $\alpha =$ Ge and (b) $\alpha =$ Se.

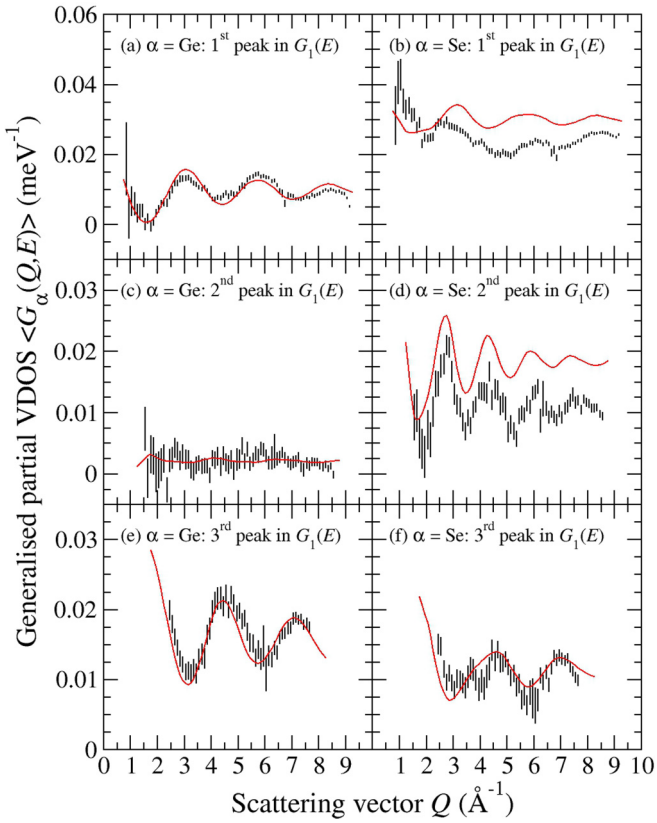

FIG. 5. The $\langle G_\alpha(Q, E)\rangle$ functions for vitreous $GeSe_2$, where the average extends over a range of energies corresponding to (a) and (b) the first peak, (c) and (d) the second peak, and (e) and (f) the third peak in $G_1(E)$ (Fig. 3). The measured functions (points with vertical error bars) are compared to those obtained from a first-principles model (solid red curves). Peaks in the modeled functions are shifted to smaller energies compared to experiment, so the integration ranges are 8–18, 23–28, and 32–40 meV for experiment versus 6–16, 20–25, and 28–36 meV for the model.

VI. FIRST-PRINCIPLES MODEL

A 180-atom model for the glass was generated using classical molecular dynamics with the interatomic potentials from [31,32] and a quench-from-the-melt protocol. The atomic coordinates of the model were then optimized within a first-principles framework [33] to give a network structure in which chemical order prevails. This network is based predominantly on tetrahedral $Ge(Se_{1/2})_4$ units, in accordance with vibrational spectroscopy [29,30,34–36], with 33% of the Ge atoms in edge-sharing conformations, in accordance with diffraction [21,22]. The vibrational properties of the model were calculated within the harmonic approximation through a density-functional-based finite-difference scheme [9,10,33], and the $Z_\alpha(E)$ functions were extracted (Fig. 6). The functions $G_\alpha(Q, E)$ and $G_\alpha(E)$ were also calculated for a temperature of 4 K by adopting the same approximations as used in the interpretation of the present CINS results for the same Q range accessible to the MERLIN spectrometer and by adopting the E-dependent energy resolution function of this instrument. Hence, Eq. (32) provided the starting point for extracting the $S_{\alpha\alpha}(Q, E)$ functions from the simulated $S_{\mathrm{coh},1}(Q, E)$ functions for the different isotopically enriched samples. The modeled $\langle G_\alpha(Q, E)\rangle$ and $G_\alpha(E)$ functions are shown in Figs. 5 and 6, respectively.

Figure 6 shows that the profiles of the modeled $G_\alpha(E)$ functions are similar to those found from experiment, although there is an energy downshift that is also reported in previous first-principles molecular dynamics investigations of $GeSe_2$ glass [37–40]. As per the CINS results, the model shows that the A_1 and A_1^c modes for corner- and edge-sharing tetrahedral $Ge(Se_{1/2})_4$ units originate predominantly from the motion of Se atoms [33]. These modes manifest themselves as distinctive peaks at $\simeq$24.6 and 26.7 meV, respectively, in Raman spectroscopy experiments [34–36].

Figure 5 shows that the modeled $\langle G_\alpha(Q, E)\rangle$ functions display a Q-space pseudoperiodicity that matches experiment, provided that an allowance is made for the energy downshift in the theoretical results. According to the model, these Q-space oscillations originate primarily from Ge-Se correlations. The $\langle G_{\mathrm{Se}}(Q, E)\rangle$ function of Fig. 5(d) originates from the motion of Se atoms in the second peak region of $G_1(E)$, where there is little contribution to the VDOS from the motion of Ge atoms.

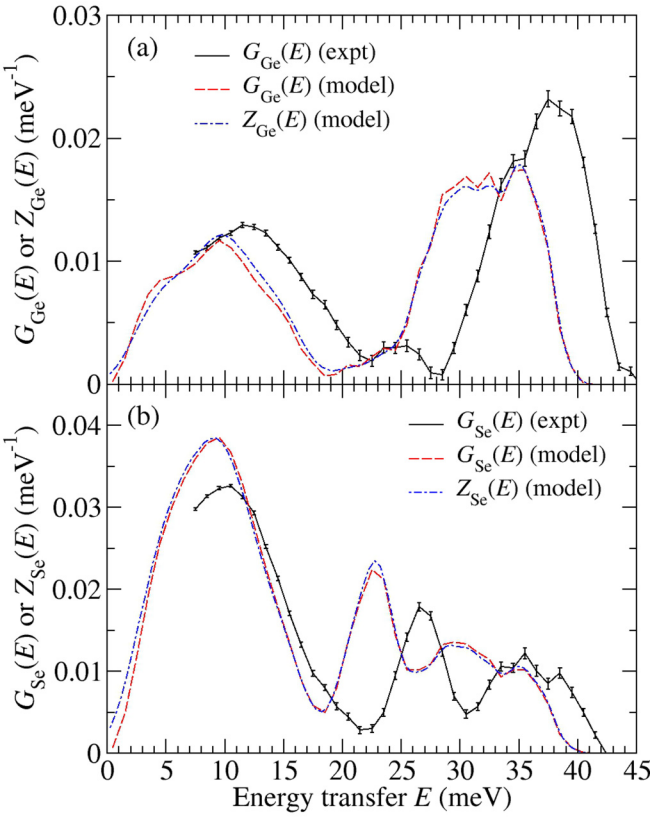

FIG. 6. The $G_\alpha(E)$ functions for (a) Ge and (b) Se for vitreous $GeSe_2$ at 5 K as measured using CINS (solid black curves with vertical error bars) or calculated using a first-principles model (dashed red curves). From experiment, there are peaks in $G_{Ge}(E)$ at 11.7(2), 24.7(1), and 38.0(1) meV and a shoulder at 35(2) meV, and there are peaks in $G_{Se}(E)$ at 9.9(1) and 26.8(1) meV followed by a broad feature with peaks at 33.8(1), 35.5(1), and 38.4(1) meV. The inelastic contribution to the measured signal could not be separated from the resolution-broadened elastic scattering at $E < 7.5$ meV. From the model, $G_\alpha(E) \simeq Z_\alpha(E)$, where the $Z_\alpha(E)$ functions are given in (a) and (b) by the dash-dotted blue curves.

The observed pseudoperiodicity of ~ 1.55 Å^{-1} is comparable to the periodicity of $2\pi/\bar{r}_{SeSe} = 1.6$ Å^{-1} calculated from the Se-Se distance $\bar{r}_{SeSe} = 3.89$ Å for tetrahedral $Ge(Se_{1/2})_4$ units [21,22]. In comparison, Fig. 6 shows that both Ge and Se atoms contribute to the vibrational modes in the first and third peak regions of $G_1(E)$. The associated $\langle G_\alpha(Q,E)\rangle$ functions, shown in Figs. 5(a), 5(b), 5(e) and 5(f), display a pseudoperiodicity of ~ 2.7 Å^{-1}, which is comparable to the periodicity of $2\pi/\bar{r}_{GeSe} = 2.67$ Å^{-1} calculated from the Ge-Se bond distance $\bar{r}_{GeSe} = 2.36$ Å for tetrahedral $Ge(Se_{1/2})_4$ units [21,22].

Overall, the first-principles model gives a good account of the vibrational properties of glassy $GeSe_2$ [33] and is sufficiently realistic to show that $G_\alpha(E) \simeq Z_\alpha(E)$, where discrepancies are small and comparable to the statistical error on the measured $G_\alpha(E)$ functions (Fig. 6). This finding demonstrates the validity of analyzing the CINS results by using a scheme in which the incoherent approximation that leads to Eq. (29) is combined with the Q-averaging procedure of Eq. (31). The latter is important because the first-principles model shows that the Q-dependent features in the measured $G_\alpha(Q,E)$ functions have a major contribution from Ge-Se correlations, along with a smaller contribution from correlations between distinct atoms of the same chemical species. For example, the calculated $S_{SeSe}(Q,E)$ function of Eq. (13) leads to Q-dependent oscillations in $G_{Se}(Q,E)$ that vanish, however, if $S_{SeSe}(Q,E)$ is separated into its contributions from self- and distinct Se atom terms, and the contribution from the distinct term is neglected. In both cases, the averaging procedure of Eq. (31) leads to $G_{Se}(E)$ functions that are in excellent agreement with $Z_{Se}(E)$. When Ge-Se correlations are mixed in, as per the solution for $S_{SeSe}(Q,E)$ obtained from the singular-value decomposition of Eq. (32), the resultant Q-dependent features in $G_{Se}(Q,E)$ are significant [Fig. 4(b)], but the averaging procedure of Eq. (31) again leads to a $G_{Se}(E)$ function that is in excellent agreement with $Z_{Se}(E)$ [Fig. 6(b)]. In short, distinct atom correlations do not provide a significant contribution to the one-phonon density of states, and the experimental procedure has the right ingredients to deliver accurate partial VDOS.

The downshift in energy of the simulated $G_\alpha(E)$ functions could originate from the procedure used to prepare the model structure and/or the density functional adopted in the first-principles framework for calculating its vibrational properties. For instance, a calculation of the vibrational properties of the diatomic molecule $^{74}Ge^{80}Se$, using the same setup as in the present work, delivers a stretching-mode frequency of 381 cm^{-1}. This value is $\sim$6% smaller than the experimental value of the vibrational constant $\omega_e = 402.7$ cm^{-1} [41], suggesting a contribution to the downshift that lies with the density functional. In comparison, several models of various sizes have been generated for amorphous $GeSe_2$ through the use of either a classical or first-principles approach, and their vibrational properties have been calculated with different density functionals [33,39]. In all cases, a downshift in vibrational frequencies is observed, which suggests a contribution to the downshift that also lies in the procedure used to generate the model structure. Here, the use of a quench-from-the-melt protocol delivers an effective quench rate that is orders of magnitude faster than in experiment, leading to amorphous models that are inherently less relaxed. There is also the possibility of a residual pressure effect [42]. Nevertheless, a full appraisal of the origin of the energy downshift is beyond the scope of the present computational work, which is aimed at testing the validity of the experimental approach.

VII. CONCLUSIONS

The double-differential cross sections measured in the CINS experiment on amorphous $GeSe_2$ have a substantial contribution from coherent distinct scattering that leads to a rich landscape of features in the measured $G_\alpha(Q,E)$ functions (Fig. 4). The results show, however, that the incoherent approximation of Eq. (29), when coupled with the Q-averaging procedure of Eq. (31), delivers an accurate description of the true partial VDOS. Here, the first-principles model serves the purpose of validating the experimental approach over a broad range of energy transfers.

The experimental method delivers results that transcend those obtained from traditional CINS investigations in which the measured spectra are analyzed within the extreme incoherent approximation.

The CINS technique leads to the desired target of setting experimental benchmarks for both the partial and total VDOSs based solely on measured properties. In general, this establishment of a fully experimental procedure is crucial for exploring the nature of amorphous solids because the VDOS depends on the interatomic interactions, and can therefore be used to discriminate between conflicting theoretical models for these materials. The method is applicable to amorphous solids containing elements with isotopes for which the contrast between the coherent neutron scattering lengths is sufficiently large to enable the method of neutron diffraction with isotope substitution to be employed [13,14].

ACKNOWLEDGMENTS

The work in Bath was supported by the EPSRC via Grant No. GR/R12008/01 and by the STFC Centre for Materials Physics and Chemistry via Grant No. CMPC08105. The work in Lausanne used the computational resources of the Swiss National Supercomputing Center (CSCS). We thank T. Guidi and R. Bewley (ISIS) for assistance with the MERLIN experiments and A. Zeidler (Bath) for her help in preparing Figs. 2 and 4. P.S.S. thanks J.-B. Suck (Chemnitz) for his encouragement of the experimental work.

[1] S. R. Elliott, *Physics of Amorphous Materials*, 2nd ed. (Longman, Harlow, 1990).
[2] J.-B. Suck, Int. J. Mod. Phys. **07**, 3003 (1993).
[3] A. I. Chumakov and W. Sturhahn, Hyperfine Inter. **123-124**, 781 (1999).
[4] G. Adam and J. H. Gibbs, J. Chem. Phys. **43**, 139 (1965).
[5] S. Sastry, Nature (London) **409**, 164 (2001).
[6] J. M. Carpenter and D. L. Price, Phys. Rev. Lett. **54**, 441 (1985).
[7] D. L. Price and J. M. Carpenter, J. Non-Cryst. Solids **92**, 153 (1987).
[8] S. N. Taraskin and S. R. Elliott, Phys. Rev. B **55**, 117 (1997).
[9] J. Sarnthein, A. Pasquarello, and R. Car, Science **275**, 1925 (1997).
[10] A. Pasquarello, J. Sarnthein, and R. Car, Phys. Rev. B **57**, 14133 (1998).
[11] J. C. Phillips, J. Non-Cryst. Solids **34**, 153 (1979).
[12] M. F. Thorpe, J. Non-Cryst. Solids **57**, 355 (1983).
[13] H. E. Fischer, A. C. Barnes, and P. S. Salmon, Rep. Prog. Phys. **69**, 233 (2006).
[14] P. S. Salmon and A. Zeidler, Phys. Chem. Chem. Phys. **15**, 15286 (2013).
[15] G. L. Squires, *Introduction to the Theory of Thermal Neutron Scattering* (Cambridge University Press, Cambridge, 1978).
[16] D. L. Price and K. Sköld, in *Neutron Scattering*, edited by K. Sköld and D. L. Price, Methods in Experimental Physics Vol. 23, Part A (Academic, Orlando, 1986), Chap. 1, pp. 1–97.
[17] J.-B. Suck and H. Rudin, in *Glassy Metals II*, edited by H. Beck and H.-J. Güntherodt, Topics in Applied Physics Vol. 53 (Springer, Berlin, 1983), Chap. 7, pp. 217–260.
[18] J. Dawidowski, F. J. Bermejo, and J. R. Granada, Phys. Rev. B **58**, 706 (1998).
[19] J. M. Carpenter and C. A. Pelizzari, Phys. Rev. B **12**, 2397 (1975).
[20] A. Zeidler, P. S. Salmon, R. A. Martin, T. Usuki, P. E. Mason, G. J. Cuello, S. Kohara, and H. E. Fischer, Phys. Rev. B **82**, 104208 (2010).
[21] I. Petri, P. S. Salmon, and H. E. Fischer, Phys. Rev. Lett. **84**, 2413 (2000).
[22] P. S. Salmon and I. Petri, J. Phys.: Condens. Matter **15**, S1509 (2003).
[23] R. I. Bewley, R. S. Eccleston, K. A. McEwen, S. M. Hayden, M. T. Dove, S. M. Bennington, J. R. Treadgold, and R. L. S. Coleman, Physica B (Amsterdam, Neth.) **385-386**, 1029 (2006).
[24] V. F. Sears, Neutron News **3**, 26 (1992).
[25] R. Osborn, R. S. Eccleston, S. M. Bennington, and B. G. B. Kitchener, Data reduction on HET and MARI, ISIS Neutron and Muon Source, Internal Report, 1995.
[26] P. F. J. Poncet, Institut Laue-Langevin, Internal Report No. 77P0139S, 1977.
[27] A. C. Hannon, M. Arai, R. N. Sinclair, and A. C. Wright, J. Non-Cryst. Solids **150**, 239 (1992).
[28] D. A. J. Whittaker, The structure and dynamics of fundamental glasses by neutron scattering techniques, Ph.D. thesis, University of Bath, 2012.
[29] U. Walter, D. L. Price, S. Susman, and K. J. Volin, Phys. Rev. B **37**, 4232 (1988).
[30] R. N. Sinclair, A. C. Wright, A. G. Clare, and A. C. Hannon, Phys. Chem. Glasses **43C**, 191 (2002).
[31] P. Vashishta, R. K. Kalia, G. A. Antonio, and I. Ebbsjö, Phys. Rev. Lett. **62**, 1651 (1989).
[32] P. Vashishta, R. K. Kalia, and I. Ebbsjö, Phys. Rev. B **39**, 6034 (1989).
[33] L. Giacomazzi, C. Massobrio, and A. Pasquarello, Phys. Rev. B **75**, 174207 (2007).
[34] P. Tronc, M. Bensoussan, A. Brenac, and C. Sebenne, Phys. Rev. B **8**, 5947 (1973).
[35] N. Kumagai, J. Shirafuji, and Y. Inuishi, J. Phys. Soc. Jpn. **42**, 1262 (1977).
[36] S. Sugai, Phys. Rev. B **35**, 1345 (1987).
[37] R. L. Cappelletti, M. Cobb, D. A. Drabold, and W. A. Kamitakahara, Phys. Rev. B **52**, 9133 (1995).
[38] M. Cobb, D. A. Drabold, and R. L. Cappelletti, Phys. Rev. B **54**, 12162 (1996).
[39] L. Giacomazzi, C. Massobrio, and A. Pasquarello, J. Phys.: Condens. Matter **23**, 295401 (2011).
[40] M. Micoulaut, A. Kachmar, M. Bauchy, S. Le Roux, C. Massobrio, and M. Boero, Phys. Rev. B **88**, 054203 (2013).
[41] B. M. Giuliano, L. Bizzocchi, R. Sanchez, P. Villanueva, V. Cortijo, M. E. Sanz, and J.-U. Grabow, J. Chem. Phys. **135**, 084303 (2011).
[42] A. Bouzid and C. Massobrio, J. Chem. Phys. **137**, 046101 (2012).